Materials Characterization 159 (2020) 110066

Contents lists available at ScienceDirect

Materials Characterization

journal homepage: www.elsevier.com/locate/matchar

Low cycle fatigue life of the alloy IN718 enhanced through surface nanostructuring

Sanjeev Kumar[a,*], K. Chattopadhyay[b], Vakil Singh[b], D.V.V. Satyanarayana[a], Vikas Kumar[a]

[a] Defence Metallurgical Research Laboratory, Hyderabad, India
[b] Department of Metallurgical Engineering, Indian Institute of Technology (Banaras Hindu University), Varanasi, India

ARTICLE INFO

Keywords:
IN718 alloy
Nanostructure
Surface mechanical attrition treatment
LCF life

ABSTRACT

Surface nanostructure was developed on the peak aged IN718 superalloy using surface mechanical attrition treatment (SMAT) and its influence was studied on low cycle fatigue (LCF) behaviour. The gauge section of LCF samples was SMATed with steel balls of 3 mm for the duration of 5 min at constant frequency of 20 kHz using StressVoyager to modify the surface. Surface grains of 36 μm were refined to ~49 to 73 nm following SMAT. Strain controlled cyclic tests were performed for the non-SMATed and SMATed samples at ± $\Delta\varepsilon_t/2$ from ± 0.50% to ± 1.0% at strain rate ($\dot{e}$) 1 × 10^{-3} s^{-1} under reversed loading (R = –1) at room temperature. LCF life of the SMATed specimen at $\Delta\varepsilon_t/2$ = ± 0.50%, was enhanced by more than twice that of the non-SMATed specimen.

1. Introduction

The alloy IN718 was developed for application at elevated temperature up to 650 °C [1,2]. Ni-base superalloys are widely used for structural components at high temperature, especially where creep and fatigue are the important deformation modes such as turbine blades and discs in gas turbine engines, because of its good oxidation resistance, high yield strength, and good weldability. It is a precipitation hardenable alloy; precipitate phases γ′ Ni_3(Al, Ti) and mainly γ″(Ni_3Nb) cause strengthening of the austenitic gamma (γ) matrix [3]. Fatigue strength of materials is one of the important factors for aerospace applications. Fatigue life is known to be affected by multiple variables such as microstructure of the surface and substrate, residual stress and surface roughness [4]. Approximately 90 present failures of engineering components occur due to fatigue [5], therefore, it is essential to modify the surface and improve the resistance against fatigue failure [6,7]. Various processes have been used for modification of surface of components, such as laser shock peening [8], conventional shot peening (SP) [9], ultrasonic shot peening (USP) [10] and SMAT [11–13] through inducement of compressive residual stress (CRS) and development of fine-grained structure in the surface region. USP is also known as SMAT that consists of impacting of shot at ultrasonic frequency and causing extensive plastic deformation in the region close to surface [14]. Fine-grained structure along with CRS induced in the uppermost region of surface retards the process of fatigue cracks initiation and propagation [15].

Several reports have been made on fatigue life of aluminium alloys, steels, titanium alloys and superalloys following shot peening [7,16–18]. Klotz et al. [19] observed higher fatigue strength in the shot-peened Inconel IN718 due to slow process of crack initiation. Prevey et al. [20] found increase in cyclic life of alloy Ti-6Al-4Vand IN718 at room temperature from grain refinement and inducement of CRS by shot peening. Zhao et al. [21] studied impact of SP on fatigue behaviour of the GH4169 superalloy at RT, 350 and 650 °C in air and reported that fatigue life was enhanced from the change in the process of fatigue crack initiation and propagation.

However, little attention has been paid on the role of SMAT on fatigue crack initiation and propagation in the alloy IN718, following surface modification. This investigation deals with influence of SMAT on surface microstructure and LCF behaviour of the IN718 alloy at room temperature.

2. Experimental details

Alloy IN718 was obtained from M/s Mishra Dhatu Nigam Limited, Hyderabad, as hot rolled and annealed rod of 10 mm dia. Its chemical composition is presented in Table 1. Blanks of 10 mm dia. and 110 mm long were solution treated at 980 °C for 1 h and cooled in air to room temperature (RT). Thereafter, solution treated blanks were given peak ageing treatment (720 °C for 8 h, furnace cooled at 55 °C /h and heated

* Corresponding author.
E-mail address: sanjeevphy85@gmail.com (S. Kumar).

https://doi.org/10.1016/j.matchar.2019.110066
Received 24 August 2019; Received in revised form 6 December 2019; Accepted 7 December 2019
Available online 09 December 2019
1044-5803/

Table 1
Composition of the alloy IN718 (wt%).

Fe	Cr	Nb	Mo	Ti	Al	Mn	Si	C	Cu	S	P	Ta	Co	B	Ni
19.53	18.4	5.17	3.1	1.04	0.49	0.1	0.2	0.02	0.014	0.002	0.005	0.002	0.01	0.004	Balance

to 620 °C for 8 h, and finally cooled by forced air to RT). Peak aged blanks were SMATed for 5 min using the SMAT parameters shown in Table 2. Microstructures of the specimens were characterized through Metalux–3 optical microscopy, scanning electron microscope (FESEM Quanta 200FEG) at 30 kV, following etching with solution of 5 g $CuCl_2$, in 100 ml HCl and 100 ml ethanol. Characterization of the refined grains was carried out by TEM (TECNAI G^2 20) at 200 kV. Thin foils were prepared from the surface treated region carefully sectioned from the substrate and mechanically polished from other side of the treated surface, up to the thickness of ~50 μm, and 3 mm discs were punched out from the thinned slice. The 3 mm dia. discs were electro-polished and thinned in the solution of 530 ml methanol, 170 ml perchloric acid and 300 ml n-butanol, cooled to −30 °C, at 30 V, using a twin jet polisher (Model: Struers Tenupol 5). Phase analysis and evaluation of grain size was carried out by XRD using Cu Kα radiation of wavelength 1.5402 Å with Ni filter. The residual stress was analysed using $Sin^2\ \Psi$ method with MnKα radiation tube.

Roughness profile of surface of the treated and non-treated samples was evaluated using the roughness tester (Mitutoyo, model no. SJ410).

Table 2
Processing parameters for SMATing.

SMAT frequency (kHz)	Vibration amplitude (μm)	Shot diameter (mm)	Duration of processing (minute)
20	80	3	5

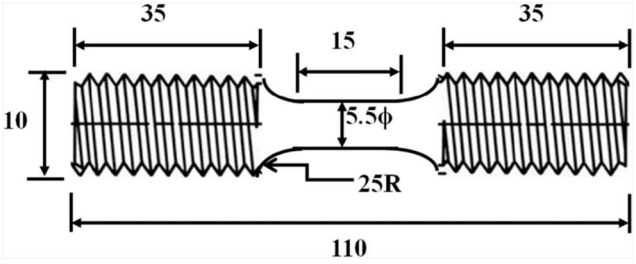

Fig. 1. Schematic geometry of the specimen used for tensile and fatigue testing.

Cylindrical fatigue samples with 5.5 mm dia. and 15 mm gauge length were fabricated from the peak aged blanks. The geometry of the sample is presented in Fig. 1. Gauge section of the fatigue samples was mechanically polished by emery papers of 400–1500 grit for removing machining marks, if any. Surface of the polished fatigue samples was subjected to mechanical attrition in a closed chamber by StressVoyager (SONATS) to modify the surface. Samples were rotated (15 rpm) during SMAT for uniform peening on the cylindrical surface.

Strain controlled fatigue tests were performed on the non-treated and surface treated samples over different $\Delta\varepsilon_t/2$ of ± 0.50%, ± 0.60%, ± 0.80% and ± 1.0%, at $1 \times 10^{-3}\ s^{-1}$ under reversed symmetrical loading ($R = -1$), using a servo-hydraulic MTS™ fatigue testing machine (Model 810). Fractography of the fatigue tested samples was carried out using SEM. All the strain controlled tests were repeated to check the reproducibility.

3. Results

3.1. Microstructural modification

Microstructure of the peak aged IN718 in the non-SMATed and SMATed condition was characterized using optical microscope, SEM and TEM. Optical micrograph of the non-SMATed sample revealed equiaxed grains of ~36 μm mean intercept length (Fig. 2). SEM micrographs showed initial microstructure of the alloy IN718 with quasi-globular and needle-like incoherent Ni_3Nb (δ-phase) particle, largely lying along the grain boundaries and some in the grains (Fig. 3). Transverse section of the SMATed sample is shown in Figs. 2b and 3b by optical and SEM micrographs, respectively. The coarse grains of the upper region of the SMATed specimen are refined up to ~200 μm depth from the treated surface. Deformation bands may also be seen in SEM micrograph of the cross-section in top region of the treated surface (Fig. 3b).These bands were developed in the top surface region following SMAT. The γ″ precipitates are uniformly distributed in the non-treated sample. The δ phase was preferentially along the grain boundaries of the austenitic matrix. It may be seen that δ and γ″ phases are of rod and disc shaped, respectively (Fig. 4a). The selected area electron diffraction (SAED) pattern of the austenitic matrix is presented in Fig. 4b. The γ″ precipitate is the main strengthening metastable phase

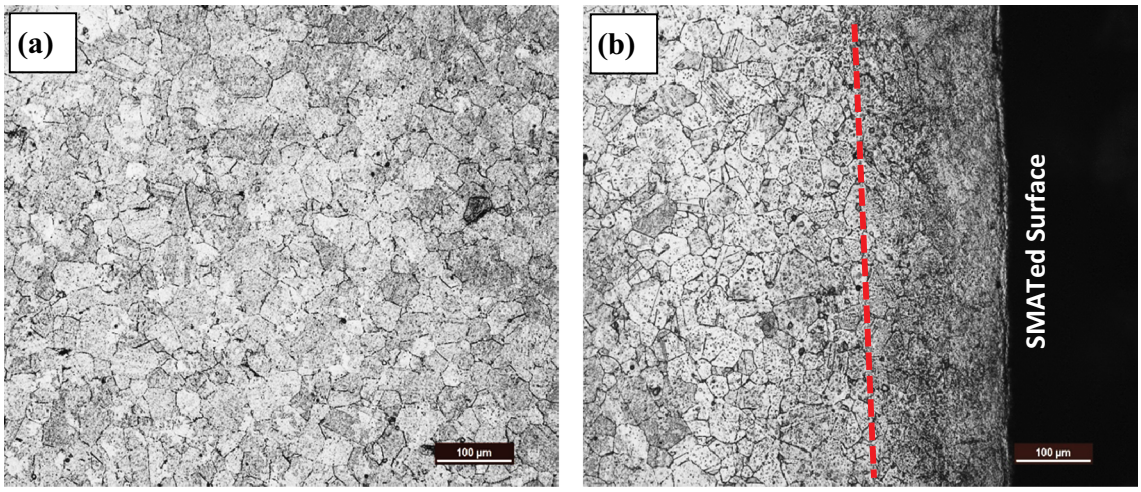

Fig. 2. Optical micrographs of the peak aged IN718: (a) non-SMATed, (b) cross-section of the SMATed sample.

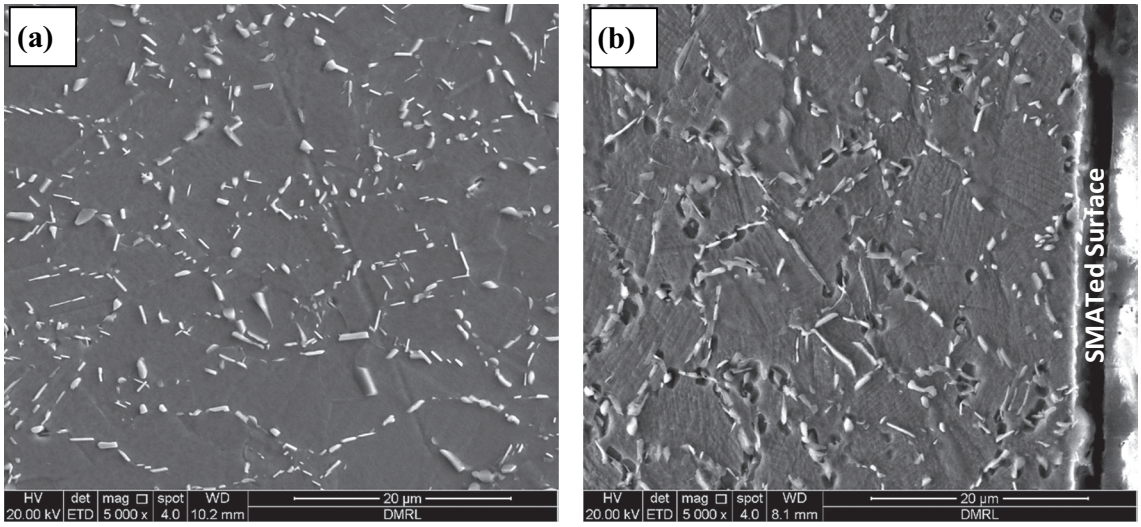

Fig. 3. SEM micrographs of the peak aged IN718: (a) non-SMATed, (b) cross-section of the SMATed sample.

in this alloy [11]. The top treated surface region is shown in the TEM micrograph (Fig. 4c). This region with refined grain is characterized by homogeneous distribution of nanostructure along with twins and shear bands in the SMATed sample. Grain refinement on the treated specimen was confirmed by partial rings in the SAED pattern (Fig. 4d). The massive spots from diffraction in the discontinuous rings of the SAED

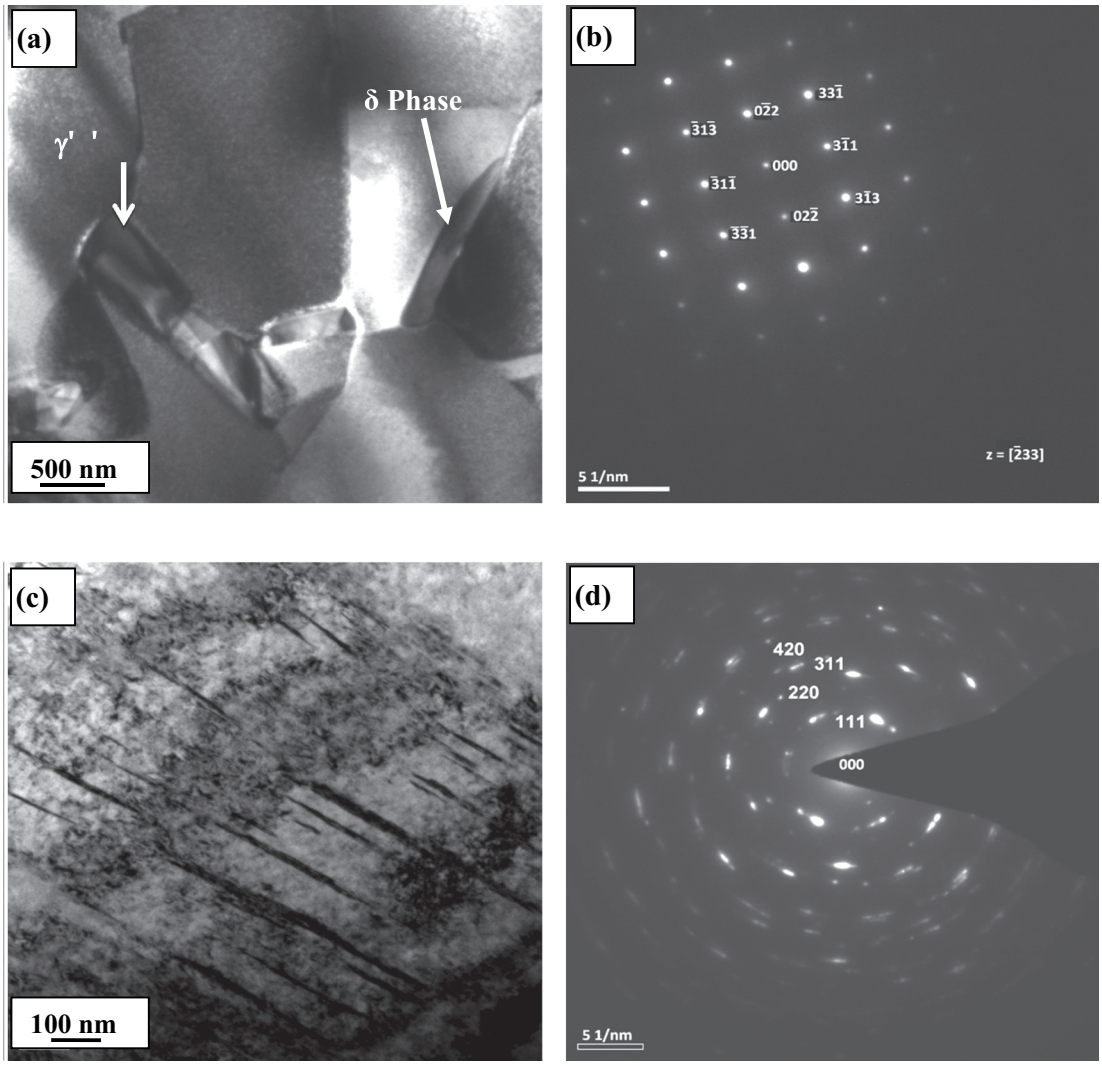

Fig. 4. TEM micrographs of the peak aged IN718 and the respective SAD patterns: (a, b) non-SMATed, (c, d) SMATed.

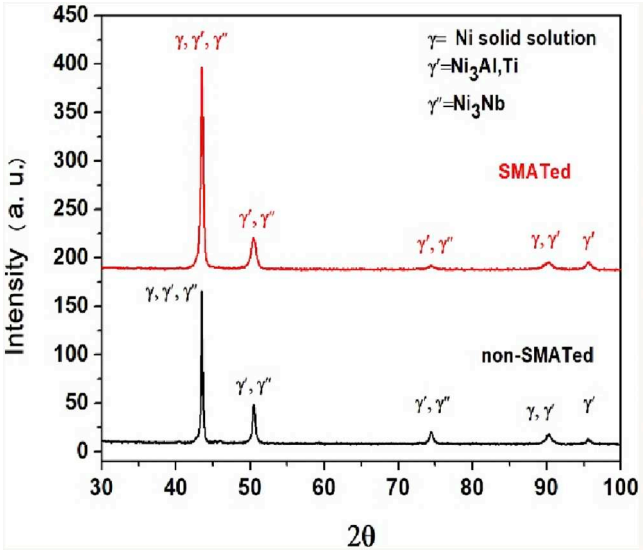

Fig. 5. X-ray diffraction of the non-SMATed and SMATed IN718 alloy.

Table 3
Surface roughness of the non-SMATed and SMATed samples of the alloy IN718.

S. No.	Treatment duration (minute)	Surface roughness (μm)		
		Ra	Rq	Rz
1.	0	0.032 ± 0.01	0.207 ± 0.007	0.522 ± 0.017
2.	5.0	1.556 ± 0.03	2.254 ± 0.032	7.732 ± 0.076

Ra = average roughness, Rq = root mean square (RMS) roughness, Rz = average maximum height of the profile.

pattern indicate a common crystallographic direction from voluminous nanograins [22]. The size of the refined grains was ~49 to 73 nm in top surface region of the SMATed sample.

3.2. XRD analysis

The microstructural phases were analysed by XRD and profiles of the non-SMATed and SMATed surface of the peak aged IN718 are presented in Fig. 5 with peaks of γ, γ′ and γ″. It may be seen that there was no phase change due to SMAT. The strengthening phases of Ni_3(Al, Ti) and Ni_3Nb with FCC and BCT crystal structure are γ′ and γ″, respectively. It may also be seen that the Bragg diffraction peaks from the treated specimen are broader than those of the non-treated one. Size of the crystallite was calculated by the Scherrer and Wilson equation [23].

$$\beta g(2\theta) = 0.9\lambda/D\cos(\theta) \quad (1)$$

where, D is the average crystallite size, θ the Bragg angle, λ the wavelength of the X-ray radiation and $\beta g(2\theta)$is peak broadening due to grain refinement in the sample. The average size of the crystallite in the treated sample was found to be ~87 nm.

3.3. Roughness

The average surface roughness (Ra) of the non-treated and treated samples was 0.032 ± 0.01 and 1.556 ± 0.03 respectively. The Ra value was determined by profilometer and was increased following the surface treatment (Table 3). The profile of the roughness surface is displayed in Fig. 6.

3.4. Residual stresses

The compressive residual stress (CRS) was analysed by Sin^2 Ψ method [24]. The residual stress peak was observed at the Bragg angle (2θ) = 151.2° on the plane (311). The compressive residual stress was 773 MPa in top surface region of the treated samples.

3.5. Low cycle fatigue (LCF)

Strain controlled cyclic tests were conducted for the non-treated as well as surface treated samples at RT at varying $\Delta\varepsilon_t/2$ of ± 0.50%, ±

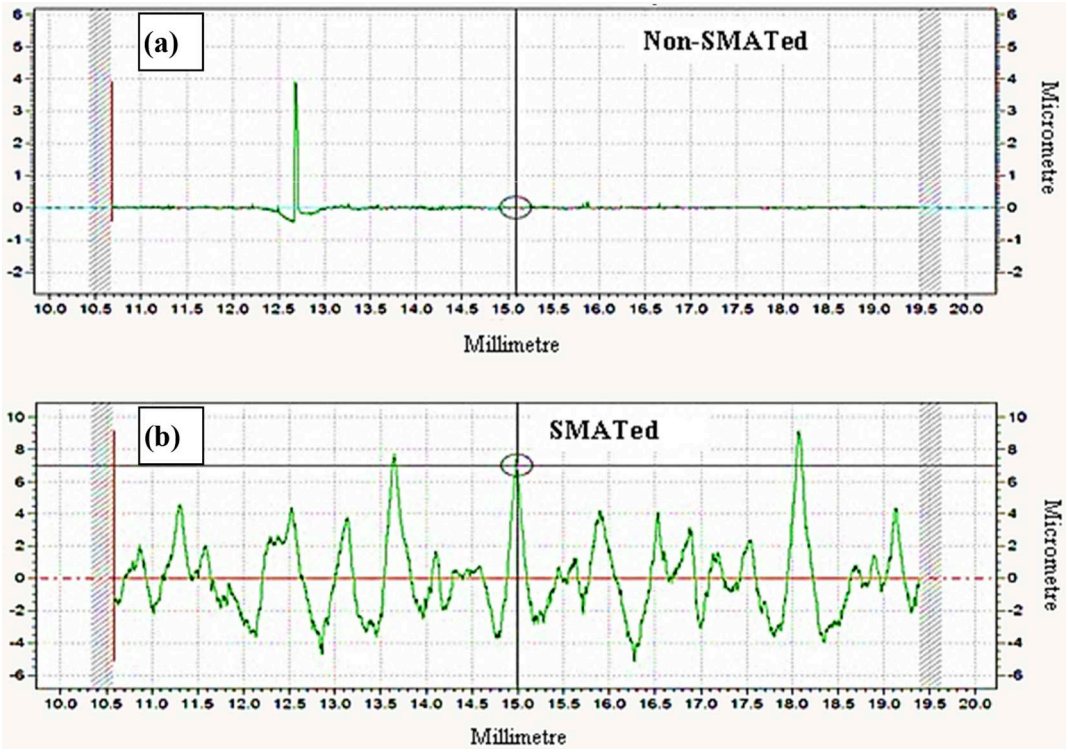

Fig. 6. Surface roughness profile: (a) non-SMATed (b) SMATed.

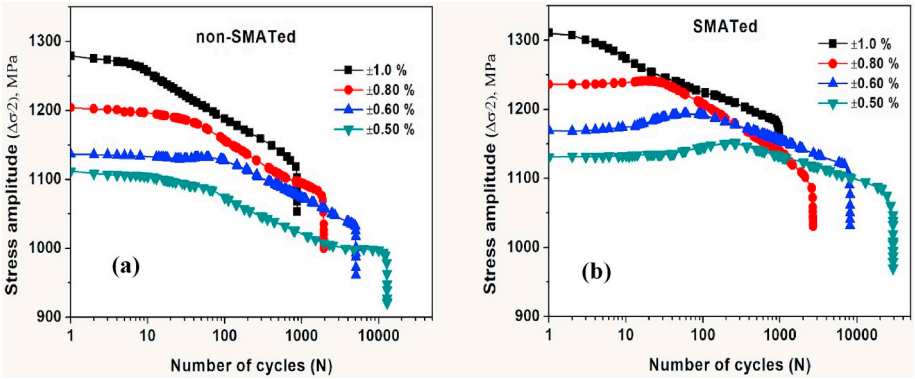

Fig. 7. Cyclic stress response at different total strain amplitudes, at constant strain rate of $1 \times 10^{-3}\ s^{-1}$: (a) non-SMATed and (b) SMATed.

0.60%, ± 0.80% and ± 1.0%. The variation of the average cyclic stress (Δσ/2) with the number of cycles (N) is displayed in Fig. 7. It shows that cyclic stress was higher in the treated sample as compared with that of the non-treated one. Continuous cyclic softening may be seen from the initial stage to failure at higher $\Delta\varepsilon_t/2$, in both the conditions. However, initial hardening up to ~50 cycles was observed at the lower strain amplitude (< ± 0.60%) in the SMATed samples. Although, at the lowest strain amplitude of ± 0.50% the hardening regime can be seen in between 100 and 300 cycles in the SMATed samples (Fig. 7b). LCF life of the non-SMATed and SMATed samples is analysed using Coffin–Mansion (C-M) equation correlating $\Delta\varepsilon_p/2$ with the number of reversal to failure ($2N_f$) [25].

$$\Delta\varepsilon_p/2 = \varepsilon'_f (2N_f)^c \quad (2)$$

where, ε'_f and c are fatigue ductility coefficient and exponent, respectively.

C-M plots of log ($\Delta\varepsilon_p/2$) vs log ($2N_f$) are shown in Fig. 8 and ε'_f and c values are presented in Table 4.

Fig. 8 shows dependence of the $2N_f$ on $\Delta\varepsilon p/2$ for the non-treated as well as the surface treated specimens. N_f gradually increases with decrease in $\Delta\varepsilon_p/2$ for both, the non-treated as well as the treated samples. The variation of fatigue life with different total strain amplitudes for non-SMATed as well as SMATed may be seen in Fig. 9. Fatigue life of the treated samples was slightly higher than those of the non-treated ones at the highest strain amplitude ($\Delta\varepsilon_t/2$ = ± 0.80%), however, it progressively increased with decrees in the $\Delta\varepsilon_t/2$ and was increased by nearly twice at the lowest strain amplitude ($\Delta\varepsilon_t/2$ = ± 0.50%). The improved fatigue life of the SMATed sample reveals the influence of surface nanostructuring and the induced CRS in the surface region.

Table 4
Numerical values of LCF parameters of the samples non-SMATed and SMATed.

Conditions	Fatigue ductility coefficient (ε'_f)	Fatigue ductility exponent (c)
Non-SMATed	0.768	−0.711
SMATed	0.411	−0.616

SEM micrographs of cylindrical surface of the fatigue tested samples in the non-treated and surface treated conditions, close to their fracture ends, are shown in Fig. 10. It is may be noticed that the size of crack is larger in the non-treated sample (Fig. 10a) with respect of those in treated sample (Fig. 10b). Fracture surface of the non-treated and the surface treated samples, tested at ± 0.50% strain amplitude, and are shown in Fig. 11. Fatigue striations are there on fracture surface of the non-treated and surface treated specimens tested at ± 0.50% strain amplitude. Initiation of multiple cracks may be seen in the non-treated and the treated sample in different areas of the fractured surfaces in different directions. Fatigue striations were observed in the non-treated fatigue tested specimen (Fig. 11b). However, tyre tracks features were observed on fracture surface of the surface treated sample (Fig. 11d).

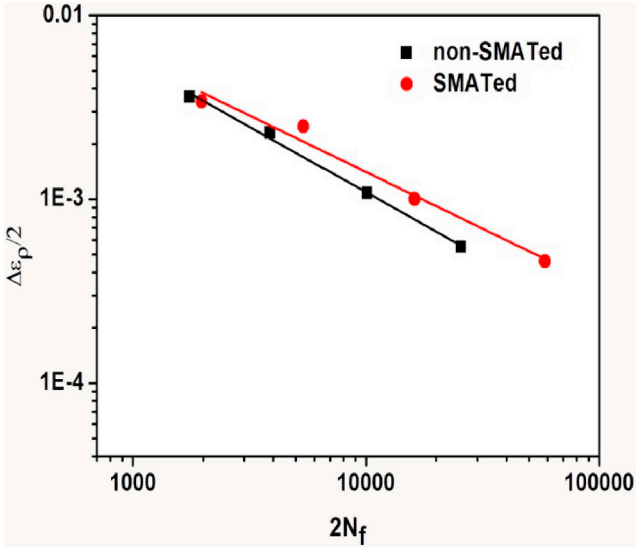

Fig. 8. Variation of reversals to failure with plastic strain amplitude, at the strain rate of $1 \times 10^{-3}\ s^{-1}$.

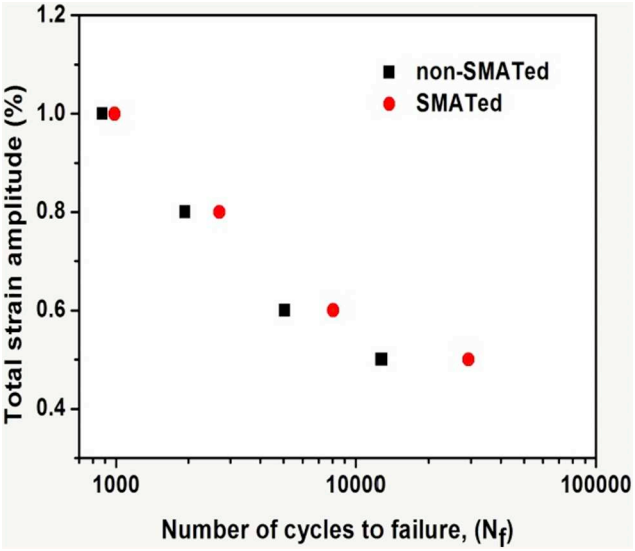

Fig. 9. Variation of LCF life with total strain amplitude.

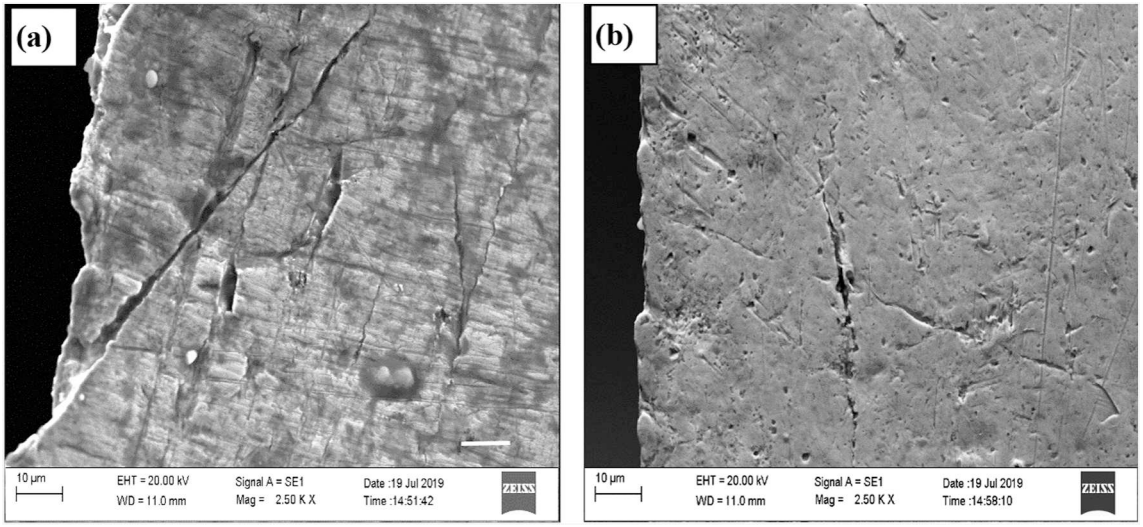

Fig. 10. SEM micrographs showing surface cracks on circumferential surface close to fracture ends of the specimen, LCF tested at ± 0.50% for: (a) non-SMATed, (b) SMATed.

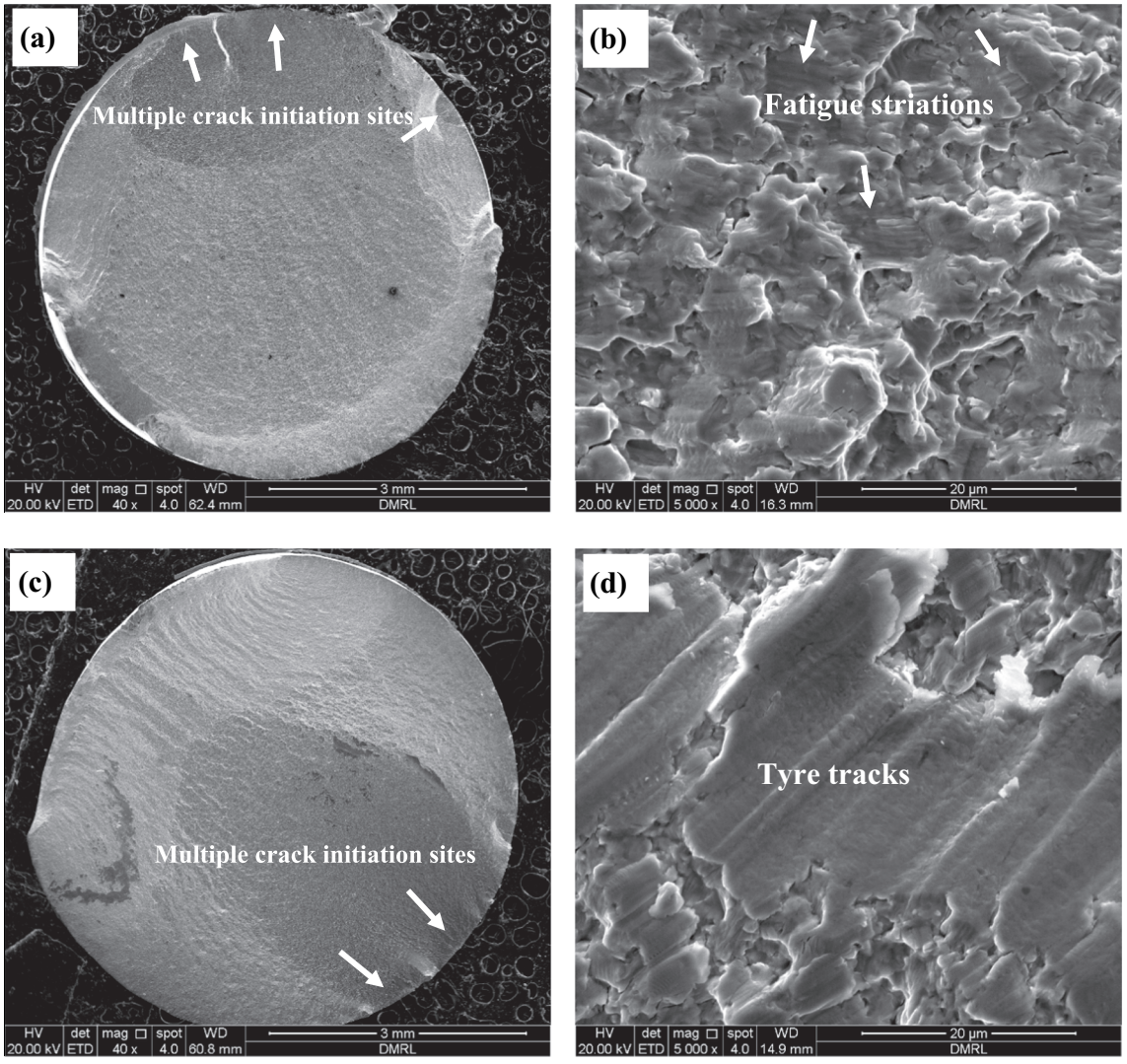

Fig. 11. Fracture behaviour of the LCF samples tested at ± 0.50% strain amplitude: (a, b) non-SMATed, (c, d) SMATed.

4. Discussion

The surface nanostructuring and deformation twins observed in the present investigation due to repeated multidirectional mechanical impacts resulted high dislocation density along with twins which is favourable for formation of sub-grains. These sub-grains have high density of dislocations and can be further refined to nano level [26]. Many processes have been used for refinement of coarse grained microstructure of metallic materials to nanoscale [4,6,8]. Refinement of the surface grains of 50–90 μm to nano size of ~16 nm in the nickel-base C-2000 alloy through severe plastic deformation at the strain rate of 1.2×10^6/s has been attributed to twinning [27]. Surface nanocrystallization in the present investigation through SMAT at similar strain rate was essentially due to the formation and intersection of twins (Fig. 4c) in line with the earlier observations [28,29].

There was no change in the phase due to SMAT (Fig. 5). Therefore, the microstructure obtained after SMAT is similar to non-SMATed condition; however, it is refined at large extent. Roughness profile of the treated specimen increased from impacts of shot media and creation of depressions and pile-ups on the surface of the sample. The increment in roughness from mechanical attrition treatment has also been reported earlier [17]. Occurrence of compressive residual stress (CRS) in the SMAT affected region is well established. It would have developed from the non-uniform elastic-plastic deformation in successive layers from the surface and the distortion of lattice caused by impact of hard steel shots on the surface [15,30,31]. The magnitude of it depends upon the process parameters of SMAT. The CRS induced in the SMAT affected surface delays the process of crack initiation as well as microcrack propagation in the affected region, reducing the effective tensile stress.

The low cycle fatigue life was enhanced from the surface treatment due to surface nanostructure and the associated CRS [32]. The cyclic stress response plots show decrease in the cyclic stress with number of cycles at all the strain amplitudes; however, cyclic stress increases with strain amplitudes, in the non-SMATed condition (Fig. 7a). The occurrence of cyclic softening in the non-SMATed condition from the very first cycle may be attributed to disordering and shearing of the strengthening precipitates of γ′ and γ″ in line with the earlier observations [33].

On the other hand cyclic hardening during the initial stage at $\Delta\varepsilon_t/2 = \pm 0.50\%$ to ± 0.80%, in the SMATed condition may be associated with disorder state of strengthening precipitates and decrease in their size in the SMAT affected region due to extensive plastic deformation. In this condition the specimen is like a composite material, consisting of inner core with order precipitates and the circumferential annual region, affected by SMAT, of nanosize grains and heavily damaged precipitates. Further, there is compressive residual stress in the SMAT affected region.

However, there was cyclic softening at the highest strain amplitude of ± 1.0% in both the conditions (Fig. 7a, b). It is due to change in the arrangement of dislocations [34]. Praveen and Singh [33] studied fatigue behaviour of the IN718 superalloy at room temperature and observed cyclic hardening followed by softening till fracture. However, initial hardening can be seen at the lower strain amplitudes in the SMATed samples. It governs the plastic deformation process which may be credited by increment in the density of dislocations. However, continuous cyclic softening behaviour may be attributed to slip and shearing of γ′ and γ″ metastable strengthening precipitates by gliding dislocations. Xiao et al. [35] and Fournier and Pineau [36] examined low cycle fatigue tested samples using transmission electron microscope and reported that softening in the alloy IN718 resulted from shearing of γ′ and γ″ strengthening precipitates. Figs. 8 and 9 show that fatigue life was improved from the surface treatment and was approximately twice at $\Delta\varepsilon_t/2 = \pm 0.50\%$. It is due to increase in resistance of the material against crack initiation because of grain refinement and the associated compressive residual stress. As revealed by SEM, multiple cracks initiated from the surface of the non-treated as well as surface treated sample tested at ± 0.50% (Fig. 11). Tyre tracks features are evident on fracture surface of treated sample (Fig. 11d). It may be noted that fatigue crack propagation occurred without formation of striations. The tyre track occurs due to fatigue crack propagation under combined action of mode-I and mode-II or mode-III. Step like features in the region of tyre tracks show crack growth on different planes. Fatigue striations result from crack growth predominantly in mode-I due to plastic blunting and sharpening at the crack tip.

5. Conclusions

Nanostructure of grain size ~49 to 73 nm developed in surface region of the peak aged IN718 alloy up to a depth of ~200 μm from SMAT with shots of 3 mm diameter. LCF life of the SMATed samples was relatively higher than those of the non-SMATed samples. LCF life of the SMATed specimen in respect of that of the non-SMATed progressively increased with decrease in the strain amplitude and the enhancement in fatigue life was nearly twice at the lowest strain amplitude of ± 0.50%. It was due to proper combination of grain refinement, surface profile and the associated compressive residual stress, in surface region of the SMATed samples.

Conflict of interest

The authors declare that they have no known competing financial interests or personal relationships that could have appeared to influence the work reported in this paper.

Acknowledgment

The authors are highly grateful to the Science and Engineering Research Board (SERB), India, for financial assistance.

References

[1] D.G. Prakash Leo, M.J. Walsh, D. Maclachlan, A.M. Korsunsky, Crack growth micro mechanisms in the IN718 alloy under the combined influence of fatigue, creep and oxidation, Int. J. Fatigue 31 (2009) 1966–1977.
[2] T.S. Byun, K. Farrell, Tensile properties of Inconel 718 after low temperature neutron irradiation, J. Nucl. Mater. 318 (2003) 292–299.
[3] Y. Huang, T.G. Langdon, Cavitation and failure in a fine-grained Inconel 718 alloy having potential superplastic properties, Mater. Sci. Eng. A 410–411 (2005) 130–133.
[4] T. Roland, D. Retraint, K. Lu, J. Lu, Fatigue life improvement through surface nanostructuring of stainless steel by means of surface mechanical attrition treatment, Scr. Mater. 54 (2006) 1949–1954.
[5] R.R. Boyer, An overview on the use of titanium in the aerospace industry, Mater. Sci. Eng. A 213 (1996) 103–114.
[6] U. Zupanc, J.G. Slovenia, Surface integrity of shot peened aluminium alloy 7075-T651, Aust. J. Mech. Eng. 57 (2011) 379–384.
[7] K. Oguri, Fatigue life enhancement of aluminum alloy for aircraft by fine particle shot peening (FPSP), J. Mater. Process. Technol. 211 (2011) 1395–1399.
[8] Y. Shadangi, K. Chattopadhyay, S.B. Rai, V. Singh, Effect of LASER shock peening on microstructure, mechanical properties and corrosion behavior of interstitial free steel, Surf. Coat. Technol. 280 (2015) 216–224.
[9] D. Gallitelli, V. Boyer, M. Gelineau, Y. Colaitis, E. Rouhaud, D. Retraint, R. Kubler, M. Desvignes, L. Barrallier, Simulation of shot peening: from process parameters to residual stress fields in a structure, C.R. Mec. 344 (2016) 355–374.
[10] S. Kumar, K. Chattopadhyay, V. Singh, Effect of ultrasonic shot peening on LCF behavior of the Ti-6Al-4V alloy, J. Alloys Compd. 724 (2017) 187–197.
[11] A. Bisht, S. Gaddam, L. Kumar, B.P. Dileep, S. Suwas, Precipitation behavior of IN718 after surface mechanical attrition treatment (SMAT) and its effect on wear properties, J. Miner. Met. Mater. Soc. 17 (2018) 2667–2776.
[12] H.W. Zhang, Z.K. Hei, G. Liu, J. Lu, K. Lu, Formation of nanostructured surface layer on AISI 304 stainless steel by means of surface mechanical attrition treatment, Acta Mater. 51 (2003) 1871–1881.
[13] B. Arifvianto, D. Suyitno, M. Mahardika, Effects of surface mechanical attrition treatment (SMAT) on a rough surface of AISI 316L stainless steel, Appl. Surf. Sci. 258 (2012) 4538–4543.
[14] Q. Sun, Q. Han, R. Xu, K. Zhao, J. Li, Localized corrosion behaviour of AA7150 after ultrasonic shot peening: corrosion depth vs. impact energy, Corros. Sci. 130 (2018) 218–230.
[15] V. Pandey, K. Chattopadhyay, N.C. Santhi Srinivas, V. Singh, Role of ultrasonic shot peening on low cycle fatigue behavior of 7075 aluminium alloy, Int. J. Fatigue 103 (2017) 426–435.

[16] Z. Sun, D. Retraint, T. Baudin, A.L. Helbert, F. Brisset, M. Chemkhi, J. Zhou, P. Kanouté, Experimental study of microstructure changes due to low cycle fatigue of a steel nanocrystallised by surface mechanical attrition treatment (SMAT), Mater. Charact. 124 (2017) 117–121.
[17] S. Kumar, K. Chattopadhyay, V. Singh, Effect of surface nanostructuring on corrosion behavior of Ti–6Al–4V alloy, Mater. Charact. 121 (2016) 23–30.
[18] Y.H. Chen, C.H. Jiang, Effect of shot peening on surface characteristics of Ni-based single-crystal superalloy, Mater. Trans. 54 (2013) 1894–1897.
[19] T. Klotz, M. Levesque, M. Brochu, Effect of rolled edges on the fatigue life of shot peened Inconel 718, J. Mater. Process. Technol. 263 (2019) 276–284.
[20] P.S. Prevey, D.J. Hornbach, P.W. Mason, Thermal Residual Stress Relaxation and Distortion in Surface Enhanced Gas Turbine Engine Components, Heat Treating: Proceedings of the 17th Conference, ASM International, 1997, pp. 3–12.
[21] X. Zhao, H. Zhao, Y. Liu, Effect of shot peening on the fatigue properties of nickel-based superalloy at high temperature, Res. Phys. 11 (2018) 452–460.
[22] T. Wang, J. Yu, B. Dong, Surface nanocrystallization induced by shot peening and its effect on corrosion resistance of 1Cr18Ni9Ti stainless steel, Surf. Coat. Technol. 200 (2006) 4777–4781.
[23] H.P. Klug, L.E. Alexander, X-Ray Diffraction Procedures for Polycrystalline an Amorphous Materials, 2nd ed, New York Wiley, 1974, p. 661.
[24] D. Delbergue, M. Levesque, P. Bocher, About the Importance of X-Ray Elastic Constant Determination in the Precise Measurement of Residual Stress Profiles, Shot Peening Performance Proceedings, 3 (2017) (237–234.
[25] G.E. Dieter, Mechanical Metallurgy, McGraw-Hill book Company, Singapore, 1988, pp. 390–391.
[26] G. Liu, J. Lu, K. Lu, Surface nanocrystallization of 316L stainless steel induced by ultrasonic shot peening, Mater. Sci. Eng. A 286 (2000) 91–95.
[27] J.C. Villegas, L.L. Shaw, Nanocrystallization process and mechanism in a nickel alloy subjected to surface severe plastic deformation, Acta Mater. 57 (2009) 5782–5795.
[28] N.R. Tao, X.L. Wu, M.L. Sui, J. Lu, K. Lu, Grain refinement at the nanoscale via mechanical twinning and dislocation interaction in a nickel-based alloy, J. Mater. Res. 19 (2004) 1623–1629.
[29] S. Kumar, G.S. Rao, K. Chattopadhyay, G.S. Mahobia, N.C.S. Srinivas, V. Singh, Effect of surface nanostructure on tensile behavior of superalloy IN718, Mater. Des. 62 (2014) 76–82.
[30] B.X. Feng, X.N. Mao, G.J. Yang, L.L. Yu, X.D. Wu, Residual stress field and thermal relaxation behavior of shot-peened TC4-DT titanium alloy, Mater. Sci. Eng. A 512 (2009) 105–108.
[31] S. Benaafia, D. Retraint, S.Y. Brou, B. Panicaud, J.L.G. Poussard, Influence of surface mechanical attrition treatment on the oxidation behaviour of 316L stainless steel, Corros. Sci. 136 (2018) 188–200.
[32] L. Zhu, Z. Wu, X. Hu, Y. Song, Comparative study of small crack growth behavior between specimens with and without machining-induced residual stress of alloy GH4169, J. Mech. Sci. Technol. 32 (2018) 5251–5261.
[33] K.V.U. Praveen, V. Singh, Effect of heat treatment on Coffin-Manson relationship in LCF of superalloy IN718, Mater. Sci. Eng. A 485 (2008) 352–358.
[34] G.S. Rao, S.R. Singh, V. Krsjak, V. Singh, Cyclic softening in annealed Zircaloy-2: Role of edgedislocation dipoles and vacancies, J. Nucl. Mater. 502 (2018) 154–160.
[35] L. Xiao, D.L. Chen, M.C. Chaturvedi, Cyclic deformation mechanisms of precipitation-hardened Inconel 718 superalloy, Mater. Sci. Eng. A 483 (2008) 369–372.
[36] D. Fournier, A. Pineau, Low cycle fatigue behavior of Inconel 718 at 298K and 823K, Metall. Trans. A. A8 (1977) 1095–1105.